

# Semiclassical theory of shot noise in ballistic conductors

G. Gomila

Departament d'Electrònica and CBEN, Universitat de Barcelona, Av.  
Diagonal 647, E-08028 Barcelona, Spain.

I. R. Cantalapiedra

Departament de Física Aplicada, Universitat Politècnica de  
Catalunya, Av. Dr. Marañon, 44, E-08028 Barcelona, Spain.

T. González

Departamento de Física Aplicada, Universidad de Salamanca, Plaza de la  
Merced, s/n, E-37008 Salamanca, Spain.

L. Reggiani

INFN-National Nanotechnology Laboratory and Dipartimento di Ingegneria  
dell'Innovazione, Università di Lecce, Via Arnesano s/n, I-73100 Lecce,  
Italy.

(January,11, 2002)

We work out a general theory of non-equilibrium noise properties (shot noise) of ballistic conductors which incorporates the correlations induced by both Pauli exclusion principle and long range Coulomb interaction. The theory provides a unifying scheme covering the whole range of system parameters and applied bias. In particular we investigate the transition from degenerate to nondegenerate injection conditions, from short to long samples and from low to high applied bias. The whole scenario is summarized by a phase diagram in the plane of the two relevant variables, sample length and contact chemical potential. Here different regions of physical interest can be identified thus providing general guidelines for investigating physical situations of specific interest. The predictions of the theory are fully corroborated by Monte Carlo simulations.

## I. INTRODUCTION

The study of non-equilibrium current noise (shot noise) in mesoscopic conductors is a subject of considerable attention in the recent literature (for a review on the subject see Ref. [ 1]). Being shot noise very sensitive to the microscopic correlations present in the system, it is very often used to obtain information on the microscopic interactions not available by other means, as for instance electric transport measurements. In the case of ballistic conductors this sensitivity has been used to investigate the relative influence of two fundamental physical interactions, namely, the Pauli exclusion principle and the long range Coulomb interaction.<sup>2-6</sup>

A ballistic conductor is characterized by an active region where carriers, once injected by contacts, move without suffering any scattering from contact to contact.<sup>7</sup> At zero temperature, a 3D ballistic conductor exhibits a zero value of the low frequency spectral density of current fluctuations,  $S_I(0)$ , and the well known Sharvin<sup>8</sup> contact resistance  $R_S = mv_F/(q^2 n)$ , with  $m$  being the electron effective mass,  $v_F$  the Fermi velocity,  $q$  the unit charge and  $n$  the carrier concentration inside the sample. These features are a consequence of the sharpness of the occupation function around the Fermi energy. At nonzero temperature,  $T$ , the broadening of the occupation function around the Fermi energy becomes responsible for the onset of thermal fluctuations and departures of the

resistance,  $R$ , from the Sharvin contact resistance. At equilibrium, Nyquist theorem<sup>9</sup> relates the resistance,  $R$ , and the noise as  $S_I(0) = 4k_B T/R$ , with  $k_B$  being the Boltzmann constant. In the presence of an external voltage  $V > k_B T/q$  Nyquist relation loses its validity and the noise starts exhibiting a greater sensitivity to Pauli and long range Coulomb correlations.

The first studies on the shot-noise properties of ballistic conductors, by assuming a Maxwell-Boltzmann (non-degenerate) carrier injection statistics,<sup>2,3</sup> did not incorporate the effect of Pauli correlations. Later on, the interplay between Pauli and Coulomb correlations was considered by assuming a Fermi-Dirac (degenerate) carrier injection statistics.<sup>4-6</sup> The effects of injection statistics that are an arbitrary function of energy and of fractional-type have also been addressed.<sup>10,11</sup> In spite of these efforts, a general analytical theory of shot noise in ballistic conductors including both Pauli and Coulomb correlations and covering the whole range of system parameters is still absent in the literature. Indeed, previous studies made use of a semi-analytical approach,<sup>4</sup> Monte Carlo (MC) simulations,<sup>5</sup> and an asymptotic analytical approach.<sup>6</sup> As a consequence, a complete and rigorous physical picture of the transport and noise properties of ballistic conductors is not available yet.

The aim of this work is precisely to address this issue. To this purpose we work out a general analytical semiclassical theory for the low frequency shot-noise prop-

erties of ballistic two-terminal conductors. We account for both the Pauli exclusion principle and the long range Coulomb interaction, and the theory is applied to the whole range of system parameters and external bias. In particular, the theory allows us to study in a unifying framework the transition from: (i) nondegenerate to degenerate injection conditions, (ii) short to (asymptotically) long sample lengths and, (iii) low to (asymptotically) high applied voltages.

By overcoming the limitations of previous existing theories, the present study allows us to compress into a general scheme the full scenario displayed by the shot-noise properties of two-terminal ballistic conductors. This scheme, validated and tested with a wide set of MC simulations, is believed to be of assistance in designing future investigations on an experimental and/or simulation basis.

The paper is organized as follows. In Sec. II we describe the system under study. In Sec. III we present the physical model used to describe the non-equilibrium noise properties. In Sec. IV the analytical expressions for the transport and noise properties are presented, and their validity checked by means of MC simulations. In Sec. V we propose a general scheme able to provide a systematic physical picture of the shot-noise properties of two-terminal ballistic conductors, and check its reliability by means of the developed theory. Finally, in Sec. VI we summarize the main results of the paper. The appendix is devoted to technical derivations.

## II. SYSTEM UNDER STUDY

As a model system for a two-terminal ballistic conductor, we consider the simple structure showed in Fig. 1. It consists of a lightly doped active region of length  $L$ , where injected carriers move in the total absence of scattering events, sandwiched between two highly doped contacts which act as ideal injecting contacts as specified later. The contacts and the ballistic region are taken of the same material (homodiode) or of different material (heterodiode). In the former case the band offset  $\Delta E_c \equiv U(0) - E_c^0 = U(L) - E_c^L$  (a symmetric structure is assumed for simplicity) vanishes, while in the later case it takes a finite value. The ballistic region is taken to be perfectly coupled with the contacts, thus no reflections take place at the interfaces. The contacts are assumed to be in quasiequilibrium at the given temperature, and at electrochemical potentials  $\xi_0$  and  $\xi_L$ , with  $\xi_L - \xi_0 = qV$ . The voltage drop in the contacts is assumed to be negligibly small (Ohmic contacts), and hence all the band bending occurs in the active region of the sample. Under these assumptions, the effective contact chemical potential  $\mu$ , defined as  $\mu \equiv \xi_0 - U(0) = \xi_L - U(L)$  is independent of the applied bias. Note that for the case of an homodiode  $\mu$  coincides with the contact Fermi energy,  $E_F \equiv \xi_0 - E_c^0 = \xi_0 - E_c^L$ , while for the case of an hetero-

diode one has  $\mu = E_F - \Delta E_c$ .

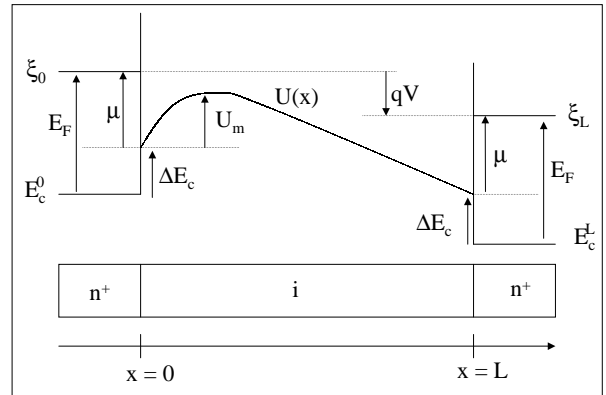


FIG. 1. Schematic band-diagram of the ballistic structure under study.

We note the existence of a maximum with amplitude  $U_m$  in the potential energy along the active region due to the presence of space charge. The structure is assumed to be sufficiently thick in the transversal directions so as to allow for a 1D electrostatic treatment. Thus the system is 1D in real space and 3D in momentum space.<sup>3</sup> The carriers are injected into the active region in accordance with the equilibrium Fermi-Dirac distribution function and satisfying the Pauli exclusion principle, thus following the corresponding binomial injection statistics.<sup>12,13</sup> For simplicity, a single spherical parabolic band is assumed.

The parameters describing the model system introduced above are therefore the length of the conductor,  $L$ , the cross sectional area  $A$ , the effective contact chemical potential,  $\mu$ , the temperature,  $T$ , the static dielectric constant of the medium,  $\epsilon$ , the electron effective mass,  $m$ , and the charge of carrier  $q$ . The independent-variable parameter is the applied voltage,  $V$ .

## III. PHYSICAL MODEL

Within a semiclassical approach the description of the transport and noise properties of the system under study can be carried out by means of the Vlasov equation, self-consistently coupled to the Poisson equation, and supplemented by appropriate *fluctuating* boundary conditions.<sup>14</sup> In the one dimensional approximation followed here, the Vlasov-Poisson system of equations reads (in dimensionless units, as specified later):

$$\left[ \frac{\partial}{\partial t} + v_x \frac{\partial}{\partial x} - \frac{\partial U(x,t)}{\partial x} \frac{\partial}{\partial v_x} \right] F(x, v_x, t) = 0 , \quad (1)$$

$$\frac{\partial^2 U(x, t)}{\partial x^2} = -n(x, t), \quad (2)$$

$$n(x, t) = \int_{-\infty}^{+\infty} dv_x F(x, v_x, t), \quad (3)$$

where  $t$  is the time variable,  $x$  the spatial coordinate,  $v_x$  the velocity in the  $x$  direction,  $U(x, t)$  the potential energy,  $F(x, v_x, t)$  the distribution function integrated over transversal momentum directions and  $n(x, t)$  the carrier density. Moreover, the boundary conditions for the potential energy read

$$U(0, t) \equiv U_0 = 0; \quad U(L, t) \equiv U_L = V, \quad (4)$$

where we have assumed that the applied bias is fixed by a low impedance external circuit so that neither the electric potential nor the contact potential energies fluctuates, i.e.,  $\delta U_0(t) = \delta U_L(t) = \delta V(t) = 0$ . Accordingly, the boundary conditions for the distribution function at the contacts read:

$$F(0, v_x, t) = \bar{F}(v_x) + \delta F_0(v_x, t); \quad v_x > 0, \quad (5)$$

$$F(L, v_x, t) = \bar{F}(v_x) + \delta F_L(v_x, t); \quad v_x < 0. \quad (6)$$

These boundary conditions consist of two contributions. The first contribution is of deterministic nature, and gives the average value of the distribution function. The second contribution is of stochastic nature, and describes the random injection of carriers. The average distribution function is given by:

$$\begin{aligned} \bar{F}(v_x) &= \int_0^{+\infty} d\varepsilon_\perp f_{FD}(\varepsilon_\perp + \varepsilon_x - \mu) \\ &= \ln(1 + e^{-\varepsilon_x + \mu}) \equiv f_c(\varepsilon_x - \mu), \end{aligned} \quad (7)$$

with  $\varepsilon_x = \frac{1}{2}v_x^2$  and  $\varepsilon_\perp = \frac{1}{2}v_\perp^2$  being the longitudinal and transversal kinetic energy, respectively, and where

$$f_{FD}(\varepsilon) = \frac{1}{1 + e^\varepsilon} \quad (8)$$

is the Fermi-Dirac distribution function. Note that due to the integration over the transverse momentum directions the effective one dimensional contact distribution function is  $f_c(\varepsilon)$  instead of  $f_{FD}(\varepsilon)$ . Moreover, the fluctuating contributions  $\delta F_0(v_x, t)$  and  $\delta F_L(v_x, t)$  have zero mean and low frequency spectral density given by<sup>6</sup>

$$\begin{aligned} 2 \int_{-\infty}^{+\infty} \overline{\delta F_a(v_x, t) \delta F_{a'}(v'_x, t')} dt = \\ \frac{\partial f_c(\varepsilon_x - \mu)}{\partial \mu} \delta_{a,a'} \delta(\varepsilon_x - \varepsilon'_x) \delta(t - t') = \\ f_{FD}(\varepsilon_x - \mu) \delta_{a,a'} \delta(\varepsilon_x - \varepsilon'_x) \delta(t - t'). \end{aligned} \quad (9)$$

Equations (1)-(9) constitute the complete set of equations to study the noise properties of the ballistic structure described in Sec. II

In the previous set of equations, and in what follows, we use dimensionless variables to simplify the notation.

The dimensionalizing factors used for energy, length, carrier density, velocity, distribution function, electric potential, electric field, electric current, resistance and current spectral density are, respectively,

$$\begin{aligned} U_0 &= k_B T; \quad L_0 = \sqrt{\frac{\epsilon k_B T}{q^2 N_0}}; \quad N_0 = 4\pi \frac{(mk_B T)^{3/2}}{h^3}; \\ v_0 &= \left(\frac{k_B T}{m}\right)^{1/2}; \quad F_0 = \frac{N_0}{v_0}; \quad V_0 = \frac{k_B T}{q}, \\ E_0 &= \sqrt{\frac{N_0 k_B T}{\epsilon}}; \quad I_0 = q A N_0 v_0; \quad R_0 = \frac{V_0}{I_0}; \quad S_{I_0} = 2qI_0, \end{aligned} \quad (10)$$

where  $h$  is the Planck constant. With this factors the dimensionless parameters describing the system are  $L/L_0 \rightarrow L$  and  $\mu/k_B T \rightarrow \mu$ , and the dimensionless independent variable is  $qV/k_B T \rightarrow V$ .

To complete our analysis, we will perform MC simulations of the system under study, so that the validity of the analytical theory can be checked by comparison. To this end we use an ensemble MC simulator, 3D in momentum space and self-consistently coupled with a 1D Poisson solver to account for Coulomb interaction. The carrier dynamics is simulated in the ballistic active region of the structure and the electron injection from the thermal reservoirs is modeled according to Fermi statistics. Due to Pauli principle, the instantaneous occupancy of an incoming electron state with energy  $\varepsilon$  and impinging at the interface between the ideal thermal reservoir and the active region fluctuates in time obeying a binomial distribution<sup>12</sup> with a probability of success given by  $f_{FD}(\varepsilon - \mu)$ . This statistics is implemented in the MC simulation of the contact injection by introducing a discretization of momentum space and using the rejection technique to select the times of injection at every momentum state.<sup>13</sup> As limiting cases, when  $\varepsilon - \mu \ll -1$ ,  $f_{FD}(\varepsilon - \mu) \cong 1$  and the injection statistics of the corresponding state is uniform in time. By contrast, when  $\varepsilon - \mu \gg 1$ ,  $f_{FD}(\varepsilon - \mu) \ll 1$  and the injection statistics is Poissonian. For the calculations we use the following parameters:  $T = 300$  K,  $m = 0.25 m_0$ ,  $\epsilon = 11.7 \epsilon_0$ , with  $m_0$  the free electron mass and  $\epsilon_0$  the vacuum permittivity.

#### IV. ANALYTICAL SOLUTION

The low frequency solution of the model presented in Sec. III can be obtained in fully analytical form. For the sake of conciseness, below we only present the final expression of the relevant quantities of interest and refer to appendix A for the details of the derivation.

### A. $I - V$ characteristics and steady-state profiles

Following the results presented in appendix A, the current voltage ( $I - V$ ) characteristics of the ballistic conductor presented in Sec. II can be calculated as

$$\bar{I} = \int_{\bar{U}_m}^{+\infty} du [f_c(u - \xi_L) - f_c(u - \xi_0)] , \quad (11)$$

where  $f_c(\varepsilon)$  is given in Eq. (7),  $\bar{U}_m$  is the average value of the maximum potential energy at applied bias  $V$ , and  $\xi_L = V + \mu$  and  $\xi_0 = \mu$  are the electrochemical potentials at the contacts located at  $x = L$  and  $x = 0$ , respectively. The value of  $\bar{U}_m$  can be calculated through the following equation (see appendix A)

$$L = \int_{\bar{U}_0}^{\bar{U}_m} \frac{dU}{E^-(U, \bar{U}_m)} - \int_{\bar{U}_L}^{\bar{U}_m} \frac{dU}{E^+(U, \bar{U}_m)} , \quad (12)$$

where

$$E^-(U, \bar{U}_m) = \left\{ \int_{\bar{U}_m}^{\infty} du \left[ \sqrt{u - U} - \sqrt{u - \bar{U}_m} \right] [f_c(u - \xi_L) + f_c(u - \xi_0)] + \int_U^{\bar{U}_m} du \sqrt{u - U} 2f_c(u - \xi_0) \right\}^{\frac{1}{2}} 2^{\frac{3}{4}} \quad (13)$$

and

$$E^+(U, \bar{U}_m) = \left\{ \int_{\bar{U}_m}^{\infty} du \left[ \sqrt{u - U} - \sqrt{u - \bar{U}_m} \right] [f_c(u - \xi_L) + f_c(u - \xi_0)] + \int_U^{\bar{U}_m} du \sqrt{u - U} 2f_c(u - \xi_L) \right\}^{\frac{1}{2}} 2^{\frac{3}{4}} . \quad (14)$$

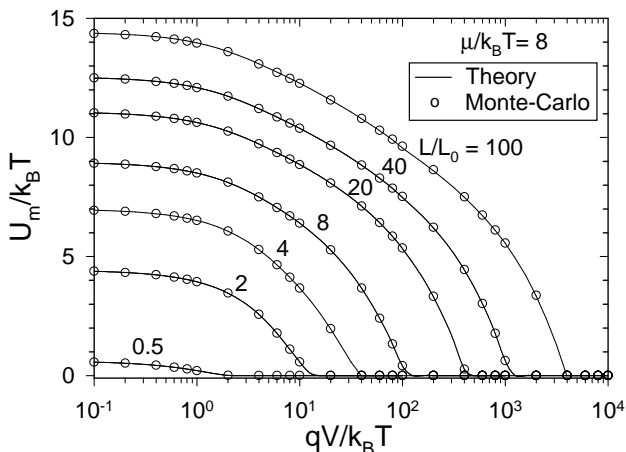


FIG. 2. Maximum energy potential  $\bar{U}_m/k_B T$  as a function of voltage for  $\mu/k_B T = 8$  and several values of the sample length  $L/L_0$ . Solid line refers to the result of the analytical calculations and open circles to those of the MC simulations.

Figure 2 reports the maximum potential energy as a function of the voltage, as calculated from Eq. (12) with  $\mu = 8$  at different values of the sample length. MC results are also shown. An excellent agreement is found between analytical and MC calculations. At vanishing voltages  $\bar{U}_m$  saturates at higher values the longer is the normalized length, because of the increasing effect of space charge inside the ballistic region. At increasing voltages  $\bar{U}_m$  starts decreasing till vanishing at a threshold voltage  $V_{cr}^m$ .

Figure 3 shows the  $I - V$  characteristics as calculated from Eq. (11) for  $\mu = 8$  and several sample lengths. The figure also reports the results of MC simulations.

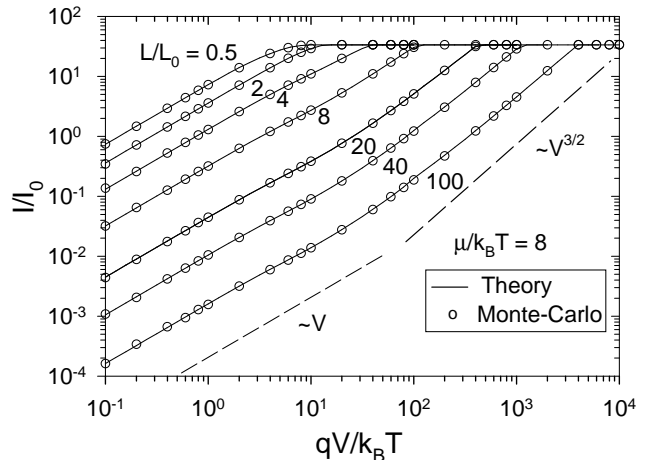


FIG. 3. I-V characteristics for  $\mu/k_B T = 8$  and several values of the sample length  $L/L_0$ . Solid lines refer to the result of the analytical calculations and open circles to those of MC simulations. Dashed curves indicate the typical power law behaviors of the Ohmic ( $V$ ) and Child-Langmuir ( $V^{3/2}$ ) regimes.

We have found perfect agreement between the results of the theory and those of MC simulations as expected, since both results are exact solutions of the same physical model. The main features of the  $I - V$  characteristics consist in the presence of a linear (Ohmic) behavior at low applied voltages and a current saturation regime at high voltages. The resistance of the linear regime is given by (in dimensionless units)

$$R_{eq} = \frac{1}{f_c(\bar{U}_m^{eq} - \mu)} . \quad (15)$$

where  $\bar{U}_m^{eq}$  is the equilibrium value of the potential energy maximum. In general, this value depends on both the sample length  $L$  and the reduced chemical potential  $\mu$ . When  $\bar{U}_m^{eq} \ll |\mu|$  the resistance takes a value independent of the sample length  $R_{eq}^{univ} = 1/f_c(-\mu)$  in agreement with the results of Ref. [15]. Typically this happens for  $L \ll 5$  and  $\mu \gg 5$ , which represent the conditions for

negligible space charge inside the ballistic region. In this limit,  $R_{eq}^{univ}$  tends to the Sharvin contact resistance  $R_S$ , as should be. The value of the saturation current is given by (in dimensionless units):

$$I_{sat} = \int_0^{+\infty} f_c(u - \mu) du . \quad (16)$$

Current saturation takes place when all carriers injected from one contact reach the opposite one, while none of the carriers injected from the other contact is able to cross the ballistic region. The value of the saturation current is independent of the sample length since it is only determined by the emission properties of the contacts. The voltage for the onset of current saturation,  $V_{cr}$ , depends on both  $L$  and  $\mu$ , as can be seen in Fig. 3. In the case that  $\mu > V_{cr}^m$ , where  $V_{cr}^m$  is the bias value at which the maximum of the potential energy disappears (see Fig. 2), one has  $V_{cr} \cong \mu + 3$ . Otherwise, when  $\mu < V_{cr}^m$ , one has  $V_{cr} = V_{cr}^m$ , and saturation coincides with the disappearance of the maximum of the potential energy. Between the linear and the current saturation regimes the  $I - V$  characteristic displays a nonlinear region, whose properties are determined by the precise values of  $L$  and  $\mu$ . The asymptotic behavior of this non-linear region for large values of  $L$  in the limit when  $\bar{U}_m \ll V < V_{cr}$  consists of a slightly sublinear region followed by a superlinear characteristic of Child-Langmuir type<sup>16</sup>  $I_{CL} = V^{3/2}/L^2$ , as has been found in Ref. [ 6]. The sublinear region is associated with a non zero temperature value that smooths out the Fermi distribution. The superlinear region is associated with space-charge effects driven by the presence of  $U_m$ .

The steady state profiles can also be calculated in closed analytical form. The potential energy profile can be obtained in inverse form from the following relations (see appendix A):

$$\int_{U_0}^{\bar{U}^-(x)} \frac{dU}{E^-(U, \bar{U}_m)} = x \quad 0 < x < \bar{x}_m , \quad (17)$$

$$\int_{U_L}^{\bar{U}^+(x)} \frac{dU}{E^+(U, \bar{U}_m)} = x - L \quad \bar{x}_m < x < L , \quad (18)$$

where  $\bar{x}_m$  is the location of the potential energy maximum inside the ballistic region. The value of  $\bar{x}_m$  can be calculated from either Eq. (17) or Eq. (18) by setting the value of  $\bar{U}(x)$  equal to  $\bar{U}_m$ . Once the potential energy profile is obtained, the electric field profile can be calculated as (see appendix A)

$$\bar{E}(x) = \begin{cases} E^-(\bar{U}^-(x), \bar{U}_m) & 0 < x < \bar{x}_m \\ E^+(\bar{U}^+(x), \bar{U}_m) & \bar{x}_m < x < L \end{cases} , \quad (19)$$

where  $E^-(U, U_m)$  and  $E^+(U, U_m)$  are given in Eqs. (13) and (14), respectively. Finally, the carrier density profile is obtained from (see appendix A)

$$\bar{n}(x) = \begin{cases} \int_{\bar{U}_m}^{+\infty} \frac{du}{\sqrt{2(u - \bar{U}^-(x))}} [f_c(u - \xi_0) + f_c(u - \xi_L)] + \\ \int_{\bar{U}^-(x)}^{\bar{U}_m} \frac{du}{\sqrt{2(u - \bar{U}^-(x))}} 2f_c(u - \xi_0); \quad 0 < x < \bar{x}_m \\ \int_{\bar{U}_m}^{+\infty} \frac{du}{\sqrt{2(u - \bar{U}^+(x))}} [f_c(u - \xi_0) + f_c(u - \xi_L)] + \\ \int_{\bar{U}^+(x)}^{\bar{U}_m} \frac{du}{\sqrt{2(u - \bar{U}^+(x))}} 2f_c(u - \xi_L); \quad \bar{x}_m < x < L \end{cases} . \quad (20)$$

Figure 4 reports the steady state profiles for  $\mu = 8$  and  $L = 8$ , at several values of the applied bias.

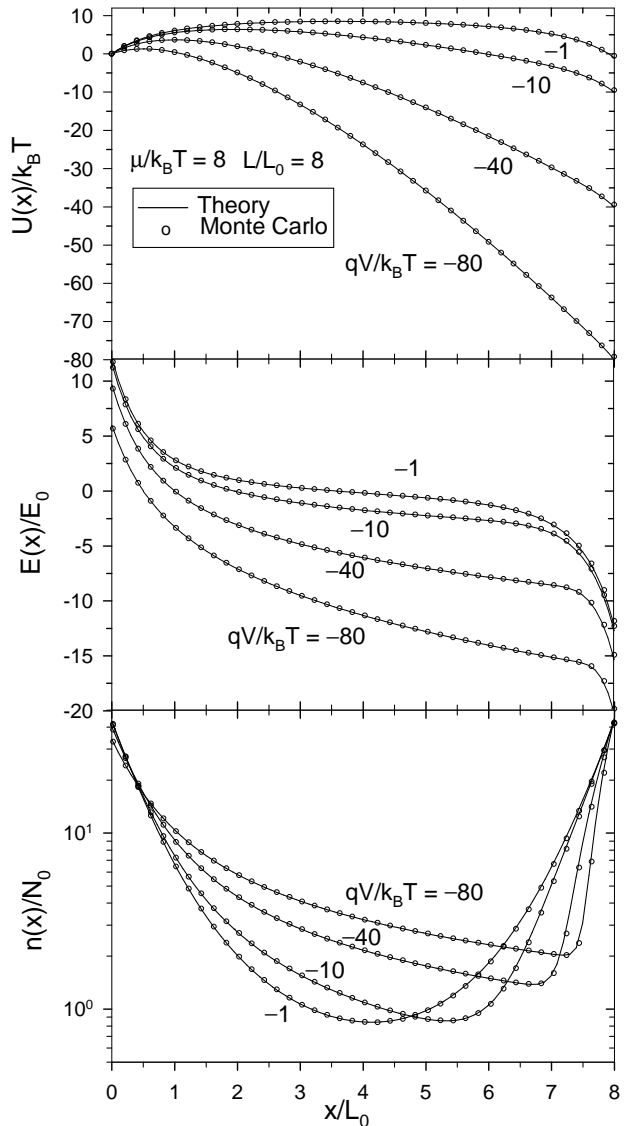


FIG. 4. Steady state profiles of the potential energy  $U(x)/k_B T$ , electric field  $E(x)/E_0$  and carrier density  $n(x)/N_0$  for  $\mu/k_B T = 8$  and  $L/L_0 = 8$ , at different values of the applied voltage  $qV/k_B T$ . Solid lines refer to the results of analytical calculations, open circles to those of MC simulations.

For the sake of comparison, the same figure also reports the profiles obtained from MC simulations. Again analytical calculations are found to perfectly agree with the simulations. The figure clearly illustrates the space-charge nature of the transport and the presence of the potential energy maximum. The value of the potential energy maximum decreases systematically at increasing bias (as already indicated in Fig. 2), while its location shifts towards the left contact. At the same time, the free charge redistributes inside the structure by shifting the minimum of the carrier density from the center of the sample towards the right contact.

## B. Noise properties

The low frequency noise properties of the system under study are characterized by the low frequency spectral density of current fluctuations defined as (in dimensionless units),

$$S_I(0) = \int_{-\infty}^{+\infty} \overline{\delta I(0)\delta I(t)} dt. \quad (21)$$

When interested in the study of the microscopic correlations the proper figure of merit is the Fano factor  $\gamma$ , which is obtained from  $S_I(0)$  as (in the dimensionless units)

$$\gamma = \frac{S_I(0)}{I} . \quad (22)$$

For conditions far from thermal equilibrium ( $V > 3$ ) a value of  $\gamma = 1$  corresponds to the absence of correlations between different current pulses, while  $\gamma < 1$  ( $\gamma > 1$ ) corresponds to the presence of negative (positive) correlations.

As shown in appendix A,  $S_I(0)$  can be calculated in closed analytical form for the model presented in Sec. III. The final result can be written in the following compact form (see appendix A)

$$S_I(0) = \int_{\overline{U}_L}^{+\infty} du [\gamma_L(u)]^2 f_{FD}(u - \xi_L) + \int_{\overline{U}_0}^{+\infty} du [\gamma_0(u)]^2 f_{FD}(u - \xi_0) , \quad (23)$$

where (see appendix A)

$$\gamma_L(u) = \begin{cases} 1 + \Omega \tilde{\gamma}^>(u) & \overline{U}_m < u < +\infty \\ \Omega \tilde{\gamma}_L^<(u) & \overline{U}_L < u < \overline{U}_m \end{cases} , \quad (24)$$

$$\gamma_0(u) = \begin{cases} -1 + \Omega \tilde{\gamma}^>(u) & \overline{U}_m < u < +\infty \\ \Omega \tilde{\gamma}_0^<(u) & \overline{U}_0 < u < \overline{U}_m \end{cases} . \quad (25)$$

Here, we have defined

$$\Omega = - \frac{[\overline{f}_c(\overline{U}_m - \xi_L) - \overline{f}_c(\overline{U}_m - \xi_0)]}{\Delta} , \quad (26)$$

with

$$\begin{aligned} \Delta = \frac{1}{\overline{E}_0} - \frac{1}{\overline{E}_L} + \int_{\overline{U}_L}^{\overline{U}_m} du \tilde{\gamma}_L^<(u) \overline{f}_{FD}(u - \xi_L) \\ + \int_{\overline{U}_0}^{\overline{U}_m} du \tilde{\gamma}_0^<(u) \overline{f}_{FD}(u - \xi_0) + \\ + \int_{\overline{U}_m}^{+\infty} du \tilde{\gamma}^>(u) [\overline{f}_{FD}(u - \xi_0) + \overline{f}_{FD}(u - \xi_L)] . \end{aligned} \quad (27)$$

Moreover,

$$\begin{aligned} \tilde{\gamma}^>(u) = \int_{\overline{U}_0}^{\overline{U}_m} dU \frac{\sqrt{2(u - U)} - \sqrt{2(u - \overline{U}_m)}}{E^-(U, \overline{U}_m)^3} \\ - \int_{\overline{U}_L}^{\overline{U}_m} dU \frac{\sqrt{2(u - U)} - \sqrt{2(u - \overline{U}_m)}}{E^+(U, \overline{U}_m)^3} , \end{aligned} \quad (28)$$

$$\tilde{\gamma}_L^<(u) = -2 \int_{\overline{U}_L}^u dU \frac{\sqrt{2(u - U)}}{E^+(U, \overline{U}_m)^3} , \quad (29)$$

$$\tilde{\gamma}_0^<(u) = 2 \int_{\overline{U}_0}^u dU \frac{\sqrt{2(u - U)}}{E^-(U, \overline{U}_m)^3} . \quad (30)$$

From the previous equations we can evaluate  $S_I(0)$  and, in turn, the Fano factor  $\gamma$ . Note that these analytical expressions are valid in the whole range of system parameters  $L$  and  $\mu$ , and in the whole range of applied bias  $V$ .

For the purpose of a reliability test, the results obtained from the analytical formulae are compared with those of MC simulations in Fig. 5. Here, the low frequency current spectral density is reported as a function of applied bias for  $\mu = 8$  and several sample lengths.

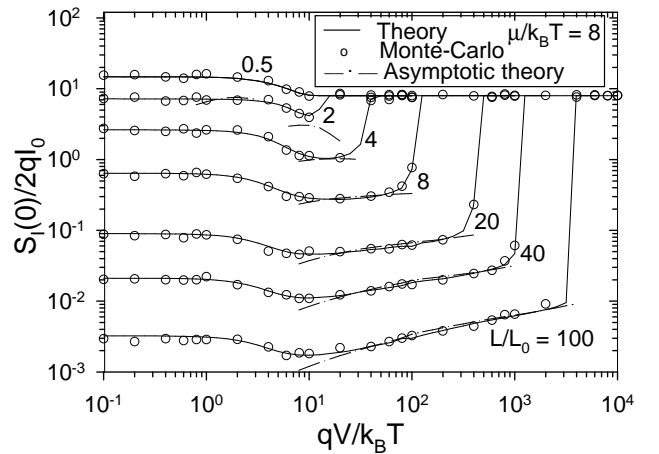


FIG. 5. Low frequency current spectral density  $S_I(0)/2qI_0$  as a function of the applied voltage  $qV/k_B T$  for  $\mu/k_B T = 8$  and several values of the sample length  $L/L_0$ . Solid lines refer to the results of analytical calculations, open circles to those of MC simulations. Dot-dashed lines are the results of the asymptotic theory.<sup>6</sup>

As can be seen in the figure, the agreement between the analytical theory and MC simulations is excellent, thus proving the reliability of both theory and simulations. For the sake of completeness Fig. 5 also reports the results obtained by means of the asymptotic theory developed in Ref. [6]. According to this theory, in the limit of  $\bar{U}_m \ll V < V_{cr}$  the low frequency current spectral density can be approximated by (in dimensionless variables)

$$S_I^{asym} = \beta(\mu - \bar{U}_m) \frac{I}{V + \bar{U}_m} , \quad (31)$$

with

$$\beta(\alpha) = 9 \left( 1 - \frac{\pi}{4} \frac{[F_{1/2}(\alpha)]^2}{F_0(\alpha)F_1(\alpha)} \right) , \quad (32)$$

where  $F_j(\alpha) = 1/\Gamma(j+1) \int_0^\infty dy y^j f_{FD}(y - \alpha)$ , with  $\Gamma(z)$  being the Gamma function. As seen in Fig. 5 the asymptotic theory agrees well with the present theory for  $\bar{U}_m \ll V < V_{cr}$ . However, it cannot describe either the transition between low and high bias regions, or the case of small sample lengths in which the condition  $\bar{U}_m \ll V < V_{cr}$  can not be satisfied.

The main features of the low frequency spectral density depicted in Fig. 5 are summarized as follows. At low voltages ( $V < 3$ ), where Ohmic conditions are satisfied,  $S_I(0)$  is bias independent and takes the value (in dimensionless variables)

$$S_I^{eq}(0) = \frac{2}{R_{eq}} = 2f_c(\bar{U}_m^{eq} - \mu) , \quad (33)$$

in agreement with Nyquist theorem.<sup>9</sup> At high voltages ( $V > V_{cr}$ ), when the sample exhibits current saturation conditions,  $S_I(0)$  is again bias independent and given by (in dimensionless variables)

$$S_I^{sat}(0) = \int_0^{+\infty} du f_{FD}(u - \xi_0) = f_c(-\mu) . \quad (34)$$

In the region of intermediate values of voltages,  $S_I(0)$  can present a monotonic or a non-monotonic behavior (with the presence of a minimum) determined by the interplay between Coulomb and Pauli correlations, as will be detailed in the next section.

## V. THE SCENARIO OF SHOT-NOISE IN BALLISTIC CONDUCTORS

The present theory enables us to investigate separately the relevance of the two mechanisms responsible for the correlations in the system under study, namely, the Pauli exclusion principle and the long range Coulomb interaction, in the whole range of system parameters. Accordingly, we propose a general scheme which summarizes the

whole scenario of the shot-noise properties exhibited by two-terminal ballistic conductors. To construct such a scheme, we make use of the Fano factor,  $\gamma$ , which is factorized into the two independent contributions,  $\gamma_P$  and  $\gamma_C$ , related to the Pauli and Coulomb correlations, respectively. Indeed, according to Eq. (9), the fluctuations of the contact distribution function at different energy levels are uncorrelated, so that the only source of correlations among carriers injected with different energy is the Coulomb interaction in the active region. As a consequence, both contributions to the Fano factor are independent, which implies  $\gamma = \gamma_P \gamma_C$ . Thus, the Pauli contribution  $\gamma_P$  corresponds to the Fano factor that would be obtained in the absence of the self-consistent long range Coulomb interaction. It can be easily evaluated from the noise calculation performed in appendix A by neglecting the self-consistent contribution. This is equivalent to set up in Eq. (23),

$$\gamma_L(u) = \begin{cases} 1 & \bar{U}_m < u < +\infty \\ 0 & \bar{U}_L < u < \bar{U}_m \end{cases} , \quad (35)$$

$$\gamma_0(u) = \begin{cases} -1 & \bar{U}_m < u < +\infty \\ 0 & \bar{U}_0 < u < \bar{U}_m \end{cases} . \quad (36)$$

For the current spectral density associated with Pauli correlations only, it is thus obtained

$$S_I^P(0) = f_c(\bar{U}_m - \xi_L) + f_c(\bar{U}_m - \xi_0) , \quad (37)$$

so that the Pauli contribution to the Fano factor is found to be

$$\gamma_P = \frac{S_I^P(0)}{\bar{I}} = \frac{f_c(\bar{U}_m - \xi_L) + f_c(\bar{U}_m - \xi_0)}{\int_{\bar{U}_m}^{+\infty} du [f_c(u - \xi_L) - f_c(u - \xi_0)]} , \quad (38)$$

where use is made of Eq. (11).

The Coulomb contribution is then evaluated as  $\gamma_C = \gamma/\gamma_P$ . According to these definitions, for  $V > 3$  values of  $\gamma_P \neq 1$  correspond to the presence of Pauli correlations, while values of  $\gamma_C \neq 1$  correspond to the presence of Coulomb correlations.

A detailed analysis of Eq. (38) indicates that the Pauli contribution is essentially dependent on the difference  $\bar{U}_m - \mu$ . Hence, when  $\bar{U}_m - \mu > 0$  it is  $\gamma_P \rightarrow 1$ , thus indicating the absence of Pauli correlations. In particular, for nondegenerate injection conditions ( $\mu < 0$ ) one always has that  $\bar{U}_m - \mu > 0$ , hence indicating the absence of Pauli correlations, as should be. By contrast, when  $\bar{U}_m - \mu < 0$  it is  $\gamma_P < 1$ , thus indicating the presence of Pauli correlations. Since  $\bar{U}_m$  is a decreasing function of the bias, the condition  $\bar{U}_m^{eq} - \mu < 0$  implies automatically that the inequality  $\bar{U}_m - \mu < 0$  is satisfied for all bias values, and hence the influence of Pauli correlations is ensured for  $V > 3$ . On the contrary, when  $\bar{U}_m^{eq} - \mu > 0$  (with  $\mu > 0$ ) Pauli correlations are absent for low (or intermediate) bias values and present for bias values sufficiently high to validate the condition  $\bar{U}_m - \mu < 0$ .

Concerning Coulomb correlations, their presence or absence is roughly determined by a value of the ratio  $L/L_{D_c}$

higher or lower than unity, respectively, where  $L_{D_c}$  is the Debye screening length corresponding to an homogeneous system with charge density equal to the equilibrium contact density. Taking into account the effects of degeneracy,  $L_{D_c}$  is calculated as (in dimensionless variables)

$$L_{D_c} = \left( \frac{dn_c^{eq}}{d\mu} \right)^{-1/2} = \frac{1}{\sqrt{2 \int_0^{+\infty} du \frac{f_{FD}(u-\mu)}{\sqrt{2u}}}} , \quad (39)$$

where we used that from Eq. (20) one has

$$n_c^{eq} = \bar{n}^{eq}(0) = 2 \int_0^{+\infty} du \frac{f_c(u-\mu)}{\sqrt{2u}} . \quad (40)$$

On the basis of these considerations, for the scenario of the shot-noise properties in ballistic conductors we propose the general scheme displayed in Fig. 6.

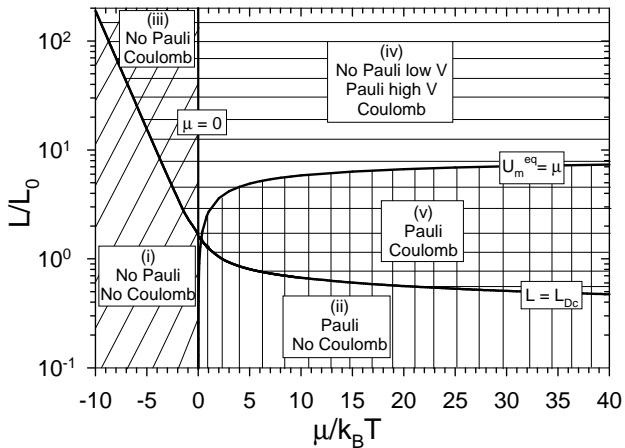


FIG. 6. Parameter plane in the length /chemical potential space representing the five different behaviours of the shot-noise properties of a ballistic conductor according to the relevance of the Pauli and Coulomb correlations. The three continuous lines define, respectively, the equalities:  $L = L_{D_c}$ ,  $\mu = 0$  and  $\bar{U}_m^{eq} = \mu$ .

In this scheme we identify five different regions in the plane  $(L, \mu)$ , corresponding to five different possibility of interplay between Coulomb and Pauli correlations. The different regions in Fig. 6 are determined by the three lines defined by the equalities  $L = L_{D_c}$ ,  $\mu = 0$  and  $\mu = \bar{U}_m^{eq}$ .

The shot noise behavior in each of the five regions corresponds, respectively, to: (i) the absence of both Pauli and Coulomb correlations ( $\mu < 0$  and  $L/L_{D_c} < 1$ ); (ii) the presence of Pauli correlations and the absence of Coulomb correlations ( $\mu > 0$ ,  $\bar{U}_m^{eq} - \mu < 0$  and  $L/L_{D_c} < 1$ ); (iii) the absence of Pauli correlations and the presence of Coulomb correlations ( $\mu < 0$  and  $L/L_{D_c} > 1$ ); (iv) the absence (presence) of Pauli correlations for low (high) bias and the presence of Coulomb correlations ( $\mu > 0$ ,  $\bar{U}_m^{eq} - \mu > 0$  and  $L/L_{D_c} > 1$ ); (v) the presence of both

Pauli and Coulomb correlations ( $\mu > 0$ ,  $\bar{U}_m^{eq} - \mu < 0$  and  $L/L_{D_c} > 1$ ).

The reliability of the above scheme has been tested by performing a series of theoretical calculations for the relevant regions identified above. We have found that the proposed scheme is essentially valid, except in the zones close to the lines separating the different regions, where intermediate behaviors have been observed. Representative examples concerning the Fano factor,  $\gamma$ , and the contributions into which it is decomposed,  $\gamma_P$  and  $\gamma_C$ , are shown in Figs. 7 to 10 for each of the five regions individuated in the  $L-\mu$  plane.

Figure 7 displays the Fano factor for  $L = 5$  and  $\mu = -5$  ( $L/L_{D_c} = 0.32$ ) corresponding to region (i) (continuous line) and for  $L = 0.5$  and  $\mu = 8$  ( $L/L_{D_c} = 0.71$ ) corresponding to region (ii) (dot-dashed line).

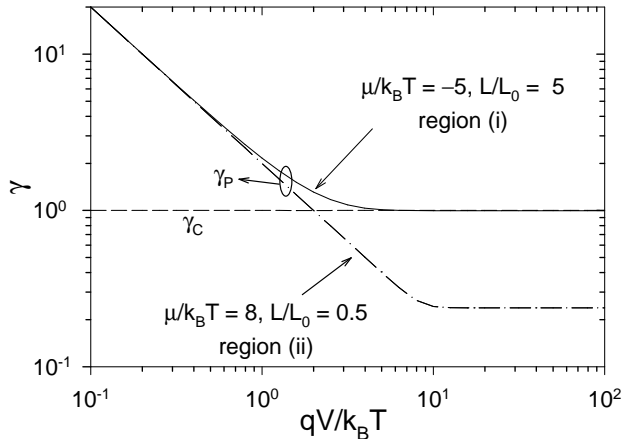


FIG. 7. Fano factor as a function of the applied voltage  $qV/k_B T$  for  $L/L_0 = 5$  and  $\mu/k_B T = -5$  corresponding to region (i) of Fig. 6 (solid line) and  $L/L_0 = 0.5$  and  $\mu/k_B T = 8$  corresponding to region (ii) of Fig. 6 (dot-dashed line). Dashed line represents the Coulomb contribution to the Fano factor. By definition, in this case the Pauli contribution to the Fano factor is indistinguishable from the actual Fano factor.

Both regions concern with the absence of Coulomb correlations ( $\gamma_C = 1$ ). However, in the former Pauli correlations play no role ( $\gamma_P = 1$  for  $V > 3$ ), while in the latter they are responsible for the suppression of shot noise ( $\gamma_P < 1$ , for  $V > 3$ ). It is worth noting that, in the absence of long range Coulomb interaction as in the present case, the Fano factor at low voltages decreases inversely with the applied bias according to the law

$$\gamma^{th} = \frac{2}{V} , \quad (41)$$

which corresponds to the thermal noise behavior, while at high voltages ( $V > V_{cr}$ ) it becomes constant with a value given by

$$\gamma^{sat} = \frac{f_c(-\mu)}{\int_0^{+\infty} f_c(u-\mu) du} , \quad (42)$$

which corresponds to current saturation conditions. To obtain Eq. (42) use is made of Eqs. (16) and (34). The value of  $\gamma^{sat}$  interpolates monotonically between 1 for  $\mu < -3$  (nondegenerate injection statistics) and  $2/\mu$  for  $\mu > 3$  (strongly degenerate injection statistics). Since the Coulomb correlations vanish identically at thermal equilibrium and under current saturation conditions, the two limiting behaviors represented by Eqs. (41) and (42) are common to all cases, as we will see below.

Figure 8 reports the Fano factor for  $L = 40$  and  $\mu = -3$  ( $L/L_{D_c} = 6.9$ ) corresponding to region (iii) of the general scheme.

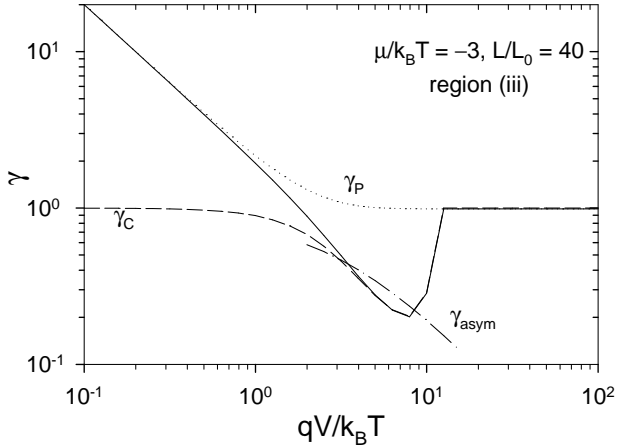


FIG. 8. Fano factor as a function of the applied voltage  $qV/k_B T$  for  $L/L_0 = 40$  and  $\mu/k_B T = -3$  corresponding to region (iii) of Fig. 6 (solid line). Dashed and dotted lines represent, respectively, the Coulomb and Pauli contributions to the Fano factor. Dashed-dotted line represents the results of the asymptotic theory.

It shows the presence of Coulomb correlations ( $\gamma_C < 1$  for  $3 < V < V_{cr}$ ) and the absence of Pauli correlations ( $\gamma_P = 1$  for  $V > 3$ ). Pauli correlations are absent because  $\mu = -3$  implies that carriers are injected at the contacts with energies  $\varepsilon - \mu > 3$ , so that the distribution function at the contacts is well approximated by the nondegenerate Maxwell-Boltzmann distribution. Due to the small value of the ratio  $L/L_{D_c}$  the asymptotic theory<sup>6</sup> provides only some rough agreement with the exact result in the limited range of voltages associated with a suppressed behavior. For larger values of the ratio  $L/L_{D_c}$  the agreement improves. The behavior displayed by the system in region (iii) was previously examined in detail in Ref. [3].

Figure 9 reports the Fano factor for  $L = 20$  and  $\mu = 8$  ( $L/L_{D_c} = 28.2$ ) corresponding to the region (iv) of the general scheme. Here we assist to a low and intermediate voltage range where Coulomb correlations are dominating and to a high voltage range where Pauli correlations prevail. Indeed, the Fano factor displays the presence of Coulomb correlations ( $\gamma_C < 1$  for  $3 < V < V_{cr}$ ), the absence of Pauli correlations in an intermediate bias range ( $\gamma_P \sim 1$  for  $3 < V \lesssim 10$ ), and the presence of Pauli

correlations for higher bias ( $\gamma_P < 1$  for  $V \gtrsim 10$ ).

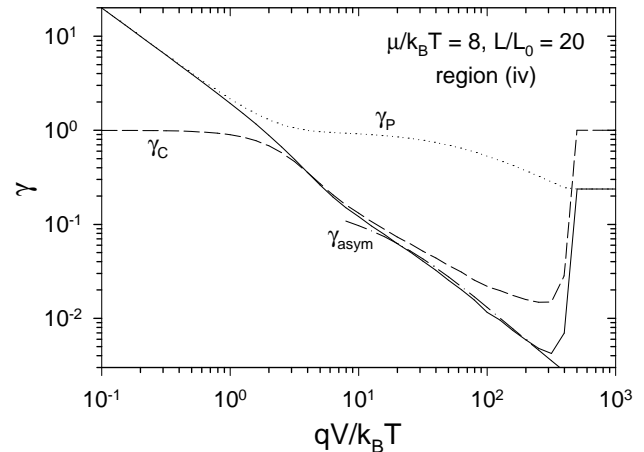


FIG. 9. Fano factor as a function of the applied voltage  $qV/k_B T$  for  $L/L_0 = 20$  and  $\mu/k_B T = 8$  corresponding to region (iv) of Fig. 6 (solid line). Dashed and dotted lines represent, respectively, the Coulomb and Pauli contributions to the Fano factor. Dashed-dotted line represents the results of the asymptotic theory.

Note that in region (iii) one has generally  $L/L_{D_c} \gtrsim 10$ , thus ensuring that the asymptotic theory<sup>6</sup> provides a good approximation to the exact theory presented here in the range of bias satisfying  $U_m \ll V < V_{cr}$ , as illustrated in Fig. 9.

Finally, Fig. 10 reports the Fano factor for  $L = 2$  and  $\mu = 8$  ( $L/L_{D_c} = 2.8$ ) corresponding to region (v) of the general scheme. The Fano factor displays the presence of both Pauli correlations ( $\gamma_P < 1$  for  $V > 3$ ) and Coulomb correlations ( $\gamma_C < 1$  for  $3 < V < V_{cr}$ ).

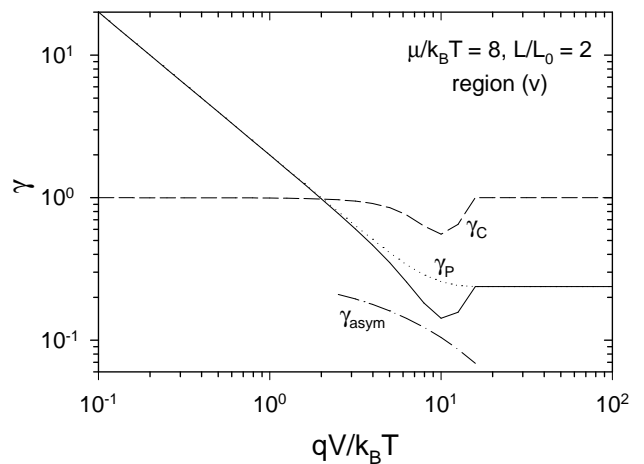


FIG. 10. Fano factor as a function of the applied voltage  $qV/k_B T$  for  $L/L_0 = 2$  and  $\mu/k_B T = 8$  corresponding to region (v) of Fig. 6 (solid line). Dashed and dotted lines represent, respectively, the Coulomb and Pauli contributions to the Fano factor. Dashed-dotted line represents the results of the asymptotic theory.

In this region one always has  $\overline{U}_m - \mu < 0$  thus ensuring that Pauli correlations are present at all applied bias. Therefore, this is the most interesting region to analyze the interplay between Coulomb and Pauli correlations. We note that here the exact theory presented in this paper becomes strictly necessary, since in this region the ratio  $L/L_{D_c}$  never takes values much higher than unity (one typically obtains  $1 \lesssim L/L_{D_c} \lesssim 10$ ), thus reducing significantly the usefulness of the asymptotic theory,<sup>6</sup> as illustrated in Fig. 10.

To provide more insight into the interplay between Coulomb and Pauli correlations in region (v), Fig. 11 reports the Fano factor as a function of bias for  $L = 3$  and several values of  $\mu$  belonging to region (v).

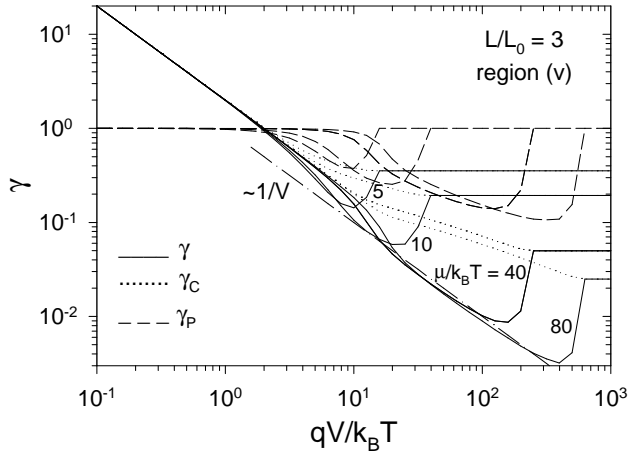


FIG. 11. Fano factor as a function of the applied voltage  $qV/k_B T$  for  $L/L_0 = 5$  and several values of  $\mu/k_B T$  corresponding to region (v) of Fig. 6 (solid line). Dashed and dotted lines represent, respectively, the Coulomb and Pauli contributions to the Fano factor. The dashed-dotted line gives the  $1/V$  slope.

It is observed that by increasing the value of  $\mu$  the contribution of the Pauli correlations decreases faster than that of the Coulomb correlations. This is understood by noting that for  $\mu > 3$ ,  $\gamma_P$  varies as  $2/\mu$ , while  $\gamma_C$ , being determined by the ratio  $L/L_{D_c}$ , varies as  $\sqrt{\mu}$ . Remarkably enough, in the region (v) for  $V > 3$  the total Fano factor  $\gamma$  is well described in all cases by a  $1/V$  dependence. As seen in the figure, this dependence on voltage is due to the joint action of both Pauli and Coulomb correlations.

To illustrate a realistic example where the theoretical results presented here could be applied, we consider as a significant example the case of a ballistic GaAs  $n^+ - i - n^+$  homodiode at  $T = 4$  K and contact density  $n_c = 1.14 \times 10^{16}$  cm $^{-3}$ . For this structure  $k_B T/q = 0.3$  mV,  $\mu = 8$  (0.24 meV),  $L_0 \sim 31$  nm and  $L_{D_c} \sim 0.7$  (22 nm), where we have taken  $m = 0.066 m_0$ , and  $\epsilon = 12.9 \epsilon_0$ . For a sample length of 500 nm,  $L \sim 16$ , and according to Fig. 6 we are in region (iv) of the general scheme. For a sample length of 70 nm,  $L \sim 2.3$  and we are in region (v). For

a sample length of 15 nm,  $L \sim 0.5$  and we are in region (ii). To explore regions (i) and (iii) one can refer to the case of heterodiodes.<sup>17</sup> We conclude that in principle the different behaviors of the Fano factor predicted by the present theory can be investigated experimentally within realistic conditions.

## VI. CONCLUSIONS

We have presented a general semiclassical theory for the noise properties of two-terminal ballistic conductors. The theory covers the whole range of system parameters and applied bias and allows one to investigate within a unitary scheme, free from any approximation, the transition between: nondegenerate and degenerate injection conditions, short and long sample lengths, low and high applied bias. Through the determination of the Fano factor, we have analyzed the relative relevance of the correlations induced by the Pauli exclusion principle and the long range Coulomb interaction. Both correlations lead to the suppression of shot noise at applied voltages above about  $3k_B T/q$ . To this purpose, we have identified five different regions in the plane defined by the sample length and the chemical potential corresponding, respectively, to: (i) the absence of Pauli and Coulomb correlations; (ii) the presence of Pauli correlations and the absence of Coulomb correlations; (iii) the absence of Pauli correlations and the presence of Coulomb correlations; (iv) the absence (presence) of Pauli correlations for low (high) bias and the presence of Coulomb correlations; and (v) the presence of both Pauli and Coulomb correlations. The results of the theory for a model conductor show a perfect agreement with analogous MC simulations. Therefore, this study, besides offering a complete physical picture of the subject, provides new insight into the noise properties of ballistic conductors, and of mesoscopic systems in general. We believe that the theory here developed constitute a powerful tool to design experimental investigations of the nonequilibrium noise properties of solid-state ballistic conductors.

## VII. ACKNOWLEDGMENTS

Partial support from the DURSI of the Generalitat de Catalunya (Spain), the Ministerio de Ciencia y Tecnología (Spain) through the projects TIC2001-1754, BFM2000-0624 and the Ramon y Cajal program, and from the Italy-Spain Joint Action of the MIUR Italy (Ref. IT-109) and MCyT Spain (Ref. HI2000-0138) is gratefully acknowledged.

## APPENDIX A: DERIVATION OF THE MAIN FORMULAE

In this appendix we derive the main formulae used in the paper by following a procedure similar to that used in Ref. [3], here extended to the case of degenerate injection conditions. To this end, the first step consists in solving for the distribution function that satisfies the Vlasov-Poisson-Langevin system of equations, Eqs. (1)-(9). To find the solution we first note that, since transport is ballistic, the total longitudinal energy of a carrier  $u$ , defined as

$$u = \frac{1}{2}v_x^2 + U(x, t) = \varepsilon_x + U(x, t), \quad (\text{A1})$$

remains constant during the flight of the carrier through the structure. Then, we note that, since transport is ballistic, carriers can reach a given point inside the structure either directly from the contacts or indirectly after reflection at the self-consistent potential barrier. Moreover, we can identify from which contact the carrier comes from. From these considerations it is easy to convince oneself that, in the low frequency limit of interest in the present paper, the distribution function solving the set of Eqs. (1)-(9) is given by

$$F(x, v_x, t) = \begin{cases} f_0(u, t) & U_0 < u < \infty, v_x > 0, 0 < x < x_m \\ f_L(u, t) & U_m < u < \infty, v_x < 0, 0 < x < x_m \\ f_0(u, t) & U_0 < u < U_m, v_x < 0, 0 < x < x_m \\ f_0(u, t) & U_m < u < \infty, v_x > 0, x_m < x < L \\ f_L(u, t) & U_L < u < U_m, v_x > 0, x_m < x < L \\ f_L(u, t) & U_L < u < \infty, v_x < 0, x_m < x < L \end{cases}, \quad (\text{A2})$$

where

$$f_0(u, t) = F\left(0, +\sqrt{2(u - U_0)}, t\right), \quad (\text{A3})$$

$$f_L(u, t) = F\left(L, -\sqrt{2(u - U_L)}, t\right), \quad (\text{A4})$$

with  $F(0, v_x, t)$  and  $F(L, v_x, t)$  obtained through the boundary conditions in Eqs. (5) and (6). In the previous expression  $U_m \equiv U_m(t)$  and  $x_m \equiv x_m(t)$  refer to the value and location of the potential energy maximum, respectively, while  $U_0$  and  $U_L$  correspond to the values of the potential energy at the contacts (note that, according to the boundary conditions assumed here, these values do not fluctuate).

Since Eq. (A2) depends on the value of the maximum potential energy, to completely determine the distribution function we need to derive the equation satisfied by the energy maximum. To this purpose, we first obtain an expression for the carrier density by performing the integral in Eq. (3) with the help of Eq. (A2). After some algebra one can show that the carrier density is given by

$$n(x, t) = \begin{cases} n^-(U(x, t), U_m; [f_0, f_L]) & 0 < x < x_m \\ n^+(U(x, t), U_m; [f_0, f_L]) & x_m < x < L \end{cases}, \quad (\text{A5})$$

where

$$\begin{aligned} n^-(U, U_m; [f_0, f_L]) = & \int_{U_m}^{+\infty} \frac{du}{\sqrt{2(u - U)}} [f_0(u, t) + f_L(u, t)] \\ & + \int_U^{U_m} \frac{du}{\sqrt{2(u - U)}} 2f_0(u, t) \end{aligned} \quad (\text{A6})$$

and

$$\begin{aligned} n^+(U, U_m; [f_0, f_L]) = & \int_{U_m}^{+\infty} \frac{du}{\sqrt{2(u - U)}} [f_0(u, t) + f_L(u, t)] \\ & + \int_U^{U_m} \frac{du}{\sqrt{2(u - U)}} 2f_L(u, t). \end{aligned} \quad (\text{A7})$$

In the previous equations the square brackets on the l.h.s. mean a functional dependence. Now, by multiplying the Poisson equation, Eq.(2), by  $\partial U(x, t)/\partial x$  and integrating with respect to  $x$ , it can be shown that the electric field  $E(x, t)$  is given through

$$E(x, t) = \begin{cases} E^-(U(x, t), U_m; [f_0, f_L]) & 0 < x < x_m \\ E^+(U(x, t), U_m; [f_0, f_L]) & x_m < x < L \end{cases}, \quad (\text{A8})$$

with

$$\begin{aligned} E^-(U, U_m; [f_0, f_L]) = & \left\{ \int_{U_m}^{\infty} du \left[ \sqrt{u - U} - \sqrt{u - U_m} \right] [f_0(u, t) + f_L(u, t)] \right. \\ & \left. + \int_U^{U_m} du \sqrt{u - U} 2f_0(u, t) \right\}^{\frac{1}{2}} 2^{\frac{3}{4}} \end{aligned} \quad (\text{A9})$$

and

$$\begin{aligned} E^+(U, U_m; [f_0, f_L]) = & \left\{ \int_{U_m}^{\infty} du \left[ \sqrt{u - U} - \sqrt{u - U_m} \right] [f_0(u, t) + f_L(u, t)] \right. \\ & \left. + \int_U^{U_m} du \sqrt{u - U} 2f_L(u, t) \right\}^{\frac{1}{2}} 2^{\frac{3}{4}}. \end{aligned} \quad (\text{A10})$$

Finally, from the definition  $\partial U(x, t)/\partial x = E(x, t)$  and its integration with respect to the space coordinate, we arrive at the following inverse equations for the potential energy profile

$$\int_{U_0}^{U^-(x, t)} \frac{dU}{E^-(U, U_m; [f_0, f_L])} = x, \quad (\text{A11})$$

valid for  $0 < x < x_m$ , and

$$\int_{U_L}^{U^+(x,t)} \frac{dU}{E^+(U, U_m; [f_0, f_L])} = x - L , \quad (\text{A12})$$

valid for  $x_m < x < L$ .

From the previous expressions the location of the maximum energy potential can be obtained by evaluating either Eq. (A11) or Eq. (A12) at  $x = x_m$ ,

$$\int_{U_0}^{U_m} \frac{dU}{E^-(U, U_m; [f_0, f_L])} = x_m , \quad (\text{A13})$$

$$\int_{U_L}^{U_m} \frac{dU}{E^+(U, U_m; [f_0, f_L])} = x_m - L . \quad (\text{A14})$$

By eliminating  $x_m$  from the two resulting equations we derive a closed equation for the value of the potential energy maximum in the form

$$L = \int_{U_0}^{U_m} \frac{dU}{E^-(U, U_m; [f_0, f_L])} - \int_{U_L}^{U_m} \frac{dU}{E^+(U, U_m; [f_0, f_L])} . \quad (\text{A15})$$

Equation (A15) constitutes a closed equation to determine the value of the potential energy maximum,  $U_m$ . Notice that it depends solely on the boundary conditions for the distribution function and the sample length.

Once the value of the potential energy maximum is known, one can determine its location through either Eq. (A13) or Eq. (A14). Then, from Eq. (A2) one obtains the explicit expression of the distribution function. In a similar way the explicit spatial dependence of the potential energy can be determined by substituting the value of  $U_m$  in Eqs. (A11) and (A12), and that of the electric field and carrier density by substituting  $U_m$  in Eq. (A8) and Eq. (A5), respectively. In this way, a complete analytical solution of the model presented in Sec. III is obtained.

In particular, the electrical current, defined as

$$I(t) = - \int_{-\infty}^{+\infty} dv_x v_x F(x, v_x, t) , \quad (\text{A16})$$

can be shown to be given by

$$I(t) = \int_{U_m}^{+\infty} du [f_L(u, t) - f_0(u, t)] . \quad (\text{A17})$$

Now, we are in the position to derive the corresponding expressions for the transport and noise properties.

### 1. Transport properties

The average steady-state transport properties can be computed directly from the equations presented above by simply substituting into them

$$\begin{aligned} U_m &\rightarrow \bar{U}_m , \\ x_m &\rightarrow \bar{x}_m , \\ f_0(u, t) &\rightarrow \bar{f}_0(u) = f_c(u - \xi_0) , \\ f_L(u, t) &\rightarrow \bar{f}_L(u) = f_c(u - \xi_L) , \end{aligned} \quad (\text{A18})$$

with  $f_c(\varepsilon)$  given through Eq. (7). In this way we arrive at the equations used in Sec. IV A

### 2. Low frequency current noise properties

The fluctuating properties of any of the quantities of interest can be evaluated directly from the equations derived above by just performing the corresponding perturbation around the steady state, and by taking into account that the only source of fluctuations in the system is located at the contacts, and represented by the fluctuating term in Eqs. (7). In this paper we are interested on the low frequency current fluctuations. To compute them we perturb Eq. (A17) around the steady state thus obtaining

$$\begin{aligned} \delta I(t) = & \int_{\bar{U}_m}^{+\infty} du [\delta f_L(u, t) - \delta f_0(u, t)] - \\ & [\bar{f}_L(\bar{U}_m) - \bar{f}_0(\bar{U}_m)] \delta U_m(t) . \end{aligned} \quad (\text{A19})$$

where  $\delta U_m(t)$  represents the fluctuations of the potential energy maximum. In the above expression we distinguish two contributions to the current fluctuation, one coming directly from the contacts and the other coming indirectly through the self-consistent potential fluctuations. To express the dependence of the second contribution on the noise sources, we perturb Eq. (A15). In performing such a perturbation it is convenient to shift all the energy integration variables by an amount equal to  $U_m$ . After some algebra one then arrives at the following expression for the fluctuations of the maximum potential energy:

$$\begin{aligned} \delta U_m(t) = & \frac{1}{\Delta} \int_{U_L}^{+\infty} du \tilde{\gamma}_L(u) \delta f_L(u, t) + \\ & \frac{1}{\Delta} \int_{U_0}^{+\infty} du \tilde{\gamma}_0(u) \delta f_0(u, t) , \end{aligned} \quad (\text{A20})$$

with

$$\begin{aligned} \Delta = & \frac{1}{\bar{E}_L} - \frac{1}{\bar{E}_0} + \int_{U_L}^{+\infty} du \tilde{\gamma}_L(u) \bar{f}_{FD}(u - \xi_L) \\ & + \int_{U_0}^{+\infty} du \tilde{\gamma}_0(u) \bar{f}_{FD}(u - \xi_0) . \end{aligned} \quad (\text{A21})$$

where we have used that  $\bar{f}'_0(u) = -\bar{f}_{FD}(u - \xi_0)$  and  $\bar{f}'_L(u) = -\bar{f}_{FD}(u - \xi_L)$ . Here, we have defined

$$\tilde{\gamma}_L(u) = \tilde{\gamma}^>(u) \theta(u - \bar{U}_m) + \tilde{\gamma}_L^<(u) \theta(\bar{U}_m - u) , \quad (\text{A22})$$

$$\tilde{\gamma}_0(u) = \tilde{\gamma}^>(u) \theta(u - \bar{U}_m) + \tilde{\gamma}_0^<(u) \theta(\bar{U}_m - u) , \quad (\text{A23})$$

with

$$\begin{aligned} \tilde{\gamma}^>(u) &= \int_{U_0}^{\bar{U}_m} \frac{\left[ \sqrt{2(u-\bar{U})} - \sqrt{2(u-\bar{U}_m)} \right] dU}{E(U, \bar{U}_m; [\bar{f}_0, \bar{f}_L])^3} \\ &- \int_{U_L}^{\bar{U}_m} \frac{\left[ \sqrt{2(u-\bar{U})} - \sqrt{2(u-\bar{U}_m)} \right] dU}{E(U, \bar{U}_m; [\bar{f}_0, \bar{f}_L])^3}, \end{aligned} \quad (\text{A24})$$

$$\tilde{\gamma}_L^<(u) = \int_{U_L}^u \frac{-2\sqrt{2(u-\bar{U})} dU}{E^+(U, \bar{U}_m; [\bar{f}_0, \bar{f}_L])^3}, \quad (\text{A25})$$

$$\tilde{\gamma}_0^<(u) = \int_{U_0}^u \frac{2\sqrt{2(u-\bar{U})} dU}{E^-(U, \bar{U}_m; [\bar{f}_0, \bar{f}_L])^3}, \quad (\text{A26})$$

By substituting Eq. (A20) in Eq. (A19) for the current fluctuations we finally obtain

$$\delta I(t) = \int_{U_L}^{+\infty} du \gamma_L(u) \delta f_L(u, t) \quad (\text{A27})$$

$$+ \int_{U_0}^{+\infty} du \gamma_0(u) \delta f_0(u, t), \quad (\text{A28})$$

with

$$\gamma_L(u) = \theta(u - \bar{U}_m) + \Omega \tilde{\gamma}_L(u), \quad (\text{A29})$$

$$\gamma_0(u) = -\theta(u - \bar{U}_m) + \Omega \tilde{\gamma}_0(u), \quad (\text{A30})$$

where

$$\Omega = -\frac{[\bar{f}_c(\bar{U}_m - \xi_L) - \bar{f}_c(\bar{U}_m - \xi_0)]}{\Delta}. \quad (\text{A31})$$

Now we are in the position to compute the low frequency current spectral density, defined as

$$S_I(0) = \int_{-\infty}^{+\infty} \overline{\delta I(0) \delta I(t)} dt. \quad (\text{A32})$$

By substituting Eq. (A27) into Eq. (A32) we arrive at

$$\begin{aligned} S_I(0) &= \int_{\bar{U}_L}^{+\infty} du \gamma_L(u)^2 f_{FD}(u - \xi_L) + \\ &\int_{\bar{U}_0}^{+\infty} du \gamma_0(u)^2 f_{FD}(u - \xi_0), \end{aligned} \quad (\text{A33})$$

where we have used that from Eq. (9) one has

$$\begin{aligned} 2 \int_{-\infty}^{+\infty} \overline{\delta f_a(u, t) \delta f_{a'}(u', t')} dt' = \\ f_{FD}(u - \xi_a) \delta_{a,a'} \delta(u - u') \delta(t - t'). \end{aligned} \quad (\text{A34})$$

From Eqs. (A24)-(A33) it is straightforward to arrive at the equations used in Sec. IV B.

<sup>1</sup> Ya. M. Blanter and M. Buttiker, Phys. Rep. **336**, 1 (2000).

<sup>2</sup> T. González, O. M. Bulashenko, J. Mateos, D. Pardo, and L. Reggiani, Phys. Rev. B **56**, 6424 (1997); O. M. Bulashenko, J. Mateos, D. Pardo, T. González, L. Reggiani, and J. M. Rubí, Phys. Rev. B **57**, 1366 (1998).

<sup>3</sup> O. M. Bulashenko, J. M. Rubí and V. A. Kochelap, Phys. Rev. B **61**, 5511 (2000).

<sup>4</sup> Y. Naveh, A. N. Korotkov, and K. K. Likharev, Phys. Rev. B **60**, R2169 (1999).

<sup>5</sup> T. González, J. Mateos, D. Pardo, and L. Reggiani, Physica B **272**, 285 (1999).

<sup>6</sup> O. M. Bulashenko and J. M. Rubí, Phys. Rev. B **64**, 045307 (2001).

<sup>7</sup> The systematic trend of downsizing the dimensions of electron devices has made possible the availability of structures where transport is controlled by the ballistic transport regime. See for instance, G. R. Facer, B. E. Kane, A. S. Dzurak, R. J. Heron, N. E. Lumpkin, R. G. Clark, L. N. Pfeiffer and K. W. West, Phys. Rev. B **59**, 4622 (1999); Zhijian Xie and S. A. Lyon, Appl. Phys. Lett. **75**, 2085 (1999); J. H. Schön, C. Kloc and B. Batlogg, J. Appl. Phys. **90**, 3419 (2001).

<sup>8</sup> Yu. V. Sharvin, Zh. Eskp. Teor. Fiz., **48**, 984 (1965); Sov. Phys. - JETP, **21**, 655 (1965).

<sup>9</sup> H. Nyquist, Phys. Rev., **32**, 110 (1928).

<sup>10</sup> O. M. Bulashenko, J. M. Rubí and V. A. Kochelap, Phys. Rev. B **62**, 8184 (2000).

<sup>11</sup> G. Gomila and L. Reggiani, Phys. Rev. B **63**, 165404 (2001).

<sup>12</sup> L. S. Levitov and G. B. Lesovik, Pis'ma Zh. Eksp. Teor. Fiz. **58**, 225 (1993) [JETP Lett. **58**, 230 (1993)].

<sup>13</sup> T. González, J. Mateos, D. Pardo, L. Varani, and L. Reggiani, Semicond. Sci. Technol. **14**, L37 (1999).

<sup>14</sup> Sh. Kogan, *Electronic Noise and Fluctuations in Solids* (Cambridge University Press, Cambridge, 1996).

<sup>15</sup> A. Greiner, L. Reggiani and L. Varani, Semicond. Sci. Technol. **15**, 1071 (2000).

<sup>16</sup> A. Van der Ziel, *Noise*, Prentice Hall Inc. (New York, 1954).

<sup>17</sup> O. M. Bulashenko, J. M. Rubí and V. A. Kochelap, Appl. Phys. Lett. **75**, 2614 (1999).